

## Chapter 5

# Surface Phonons of the 10-fold

## *d*-Al-Ni-Co

Before discussing the results of our investigations, a brief review on bulk phonons of quasicrystals is presented. Phonons in periodic crystals have well-defined energy and wavevector due to the lattice periodicity. A 3D periodic crystal having  $N$  atoms per unit cell has  $3N$  modes with three acoustic and  $3(N-1)$  optical modes. All of these modes can be characterized by using wavevectors confined to the first Brillouin zone [130].

Because of the lack of periodicity, and hence absence of a proper Brillouin zone, the wavevector cannot be a good quantum number to describe the phonon modes of quasicrystals and the concepts of periodic crystals outlined above cannot be directly employed. It has been thus of great interest to determine the vibrational properties of quasicrystals from the very beginning of their discovery. Many theoretical and experimental studies of bulk phonons and elastic properties have been carried out [73, and find references therein].

Like other properties, theoretical investigations of dynamical properties of quasicrystals began with the 1D Fibonacci sequence [131-133] and were followed by studies of Penrose tilings [134]. Dynamics of 3D quasicrystals with realistic atomic models were determined by using their higher order approximants (Refs. [135] for *i*-Al-Cu-Li, [136, 137] for *i*-Al-Zn-Mg, and [138] for *d*-Al-Mn, and [139] for a review). All of these investigations show that quasicrystals, as periodic crystals, exhibit well defined acoustic modes in the continuum limit (the long wavelength limit). The dispersion curves originate from the Bragg peaks, follow a linear relation up to a certain

wavevector, and finally become dispersionless. Since the Bragg peaks fill the reciprocal space densely, the acoustic branches in principle originate almost everywhere in  $k$ -space. However, only those phonons which are associated to the acoustic branches originating from the stronger Bragg peaks have significant intensities.

Although a Brillouin zone cannot be properly defined in quasicrystals, the positions of the stronger Bragg peaks can be considered as quasi-Brillouin-zone (QBZ) centers [140, 141]. The QBZ boundaries are packed hierarchically around the zone centers. Most of the theoretical work predicts that the acoustic branches become dispersionless at the QBZ boundaries with gaps opening. The width of the gap depends on the strength of the Bragg peaks. The calculations also show a large number of dispersionless optical branches and their density increases at higher frequencies [136].

Experimentally, the dynamics of different icosahedral and decagonal quasicrystals have been investigated by employing inelastic neutron scattering (Refs. [71, 142, 143] for *i*-Al-Pd-Mn, [144, 145] for *i*-Al-Li-Cu, [146, 147] for *i*-Al-Fe-Cu, and [72] for *d*-Al-Ni-Co) and inelastic X-ray scattering [148]. Almost all measurements confirm the theoretically predicted linear and isotropic dispersion relation. QBZ boundaries have been identified in all systems. A unique feature observed in all quasicrystals is that the phonon line width is limited by the instrumental resolution up to a certain wavevector and increases rapidly for larger wavevectors. Phonon peak broadening is thus considered as a signature of quasicrystalline ordering differing from the periodic crystals. It is believed that the continuum of dispersionless modes present in  $(\omega, k)$  space for larger energies is responsible for the peak broadening. The measured acoustic phonon peaks beyond a certain energy are just then an accumulation of contributions coming from the continuum of dispersionless modes.

The value of both  $k$ -vector and line width at which the phonon peaks start to broaden correspond to a length scale which is on the order of the size of the cluster from which the quasicrystals are made up. For example, peak broadening of transverse modes starts at around  $0.40 \text{ \AA}^{-1}$  [71] and  $0.30 \text{ \AA}^{-1}$  [72] in *i*-Al-Pd-Mn and *d*-Al-Ni-Co, respectively. The real space values of these numbers ( $2\pi$  divided by wavevector) are roughly equal to the size of the Mackay cluster (diameter =  $12 \text{ \AA}$ ) and the columnar cluster (diameter =  $20 \text{ \AA}$ ), the main building block of *i*-Al-Pd-Mn and *d*-Al-Ni-Co, respectively.

Experimental attempts to detect the theoretically predicted band gaps have not been suc-

cessful so far. Although two acoustic branches cross at the QBZ boundaries in some systems (for example see Ref. [71] for *i*-Al-Pd-Mn) where the gap is expected, no gap opening has been found. One likely reason of this may be that the gap, if present, is narrow compared to the instrumental resolution. Optical modes have been experimentally detected, particularly in *i*-Al-Pd-Mn [71, 142, 143]. The dispersionless optical modes have been observed at different energies from 8 meV to 23 meV [143].

Although the nature of the bulk phonons as discussed above have been determined, investigations of surface phonons have only just started. We have succeeded in measuring Rayleigh modes on the 10-fold surface of *d*-Al<sub>71.8</sub>Ni<sub>14.8</sub>Co<sub>13.4</sub> and the 5-fold surface of *i*-Al<sub>71.5</sub>Pd<sub>21</sub>Mn<sub>8.5</sub> by inelastic He atom scattering. Detail investigations on the surface phonons of the 10-fold *d*-Al-Ni-Co surface is carried out, which is presented in this chapter, while a brief study of the surface phonons of the 5-fold *i*-Al-Pd-Mn surface is given in the next chapter.

## 5.1 Time-of-flight Spectra

The surface phonons are measured by inelastic He atom scattering in a time-of-flight (TOF) setup. Details of the TOF technique and the experimental chamber are discussed in Chapter 2. The key idea is that the He atom beam is scattered from the surface and the time-of-flight of inelastically scattered He atoms with respect to the elastically scattered He atoms is measured (see Section 2.1.3 for details).

The surface was prepared by sputtering and annealing. The preparation conditions and quality monitoring procedures have been presented in Section 3.2. The TOF spectra were recorded at an elevated sample temperature. This has a two-fold advantage: first one is somewhat technical. The surface at room temperature contaminates very fast due to the adsorption of residual gases present in the experimental chamber. But, due to the low intensity of inelastically scattered He atoms, the measurement time of each TOF spectrum has to be fairly long (at least an hour) to observe pronounced phonon peaks. Keeping the sample at elevated temperature, the quality of surface can be maintained for a longer time, which avoids the frequent surface cleaning tasks. The second advantage is related to the thermal population of the surface phonons. At higher temperature, the population of the phonons is higher. This results in a larger probability of phonon annihilation during scattering, increasing the amplitudes of annihilation peaks.

However, at very high temperature the multiphonons are dominant over single phonons. An appropriate temperature is found at around 150-200 °C. TOF spectra were taken along the two high symmetry directions of the surface at different beam energies from 10 to 33 meV and for a large set of angles of incidence  $\theta_i$ .

Two representative TOF spectra recorded at  $\theta_i = 46.5^\circ$  and  $42.7^\circ$  are shown in Figures 5.1(a-b). They consist of a central elastic peak, phonon annihilation and creation peaks, and a broad background. The elastic peak is due to the diffuse scattering from defects. The annihilation peaks appear at lower flight time than the elastic peak due to the gain of energy during the scattering (Figure 5.1(a)). Similarly, He atoms which loose energy appear as creation peaks at higher flight time (Figure 5.1(b)). The energy and parallel momentum transfer of the phonons are calculated from the flight time, beam energy, and angle of incidence including other experimental parameters (see Section 2 for the formula).

The intensities as a function energy transfer are shown in Figures 5.1(c-d). The data were fitted by a sum of Gaussian and Lorentzian line shape for all contributions (the phonon and diffuse elastic peak and the background). The fitting was carried out by minimizing the  $\chi^2$  value ( $\chi^2 = \frac{1}{N} \sum_N [\frac{(X_N^{Exp} - X_N^{fit})^2}{\sigma_N^2}]$ ). The total fit as well as the individual elastic, inelastic, and background parts are shown in the figure. The annihilation peak at 1.8 meV has a momentum transfer  $\Delta K = -0.05 \text{ \AA}^{-1}$ , while the creation peak at -2.5 meV has  $\Delta K = 0.1 \text{ \AA}^{-1}$ . The full-width at half-Maxima (FWHM) of these peaks is about 1.2 meV, which mainly reflects the instrumental broadening.

The presence of well-defined inelastic peaks indicates that the inelastic collisions have a significant single phonon contribution. However, a non-negligible contribution from multiphonon scattering is also expected. Single phonon scattering is dominant over multiple phonons if  $2W < 1$ , where  $W$  is the surface Debye Waller factor and given by  $2W = 24(m/M)(E_{iz}/k_B\theta_D)(T/\theta_D)$ , with  $\theta_D$  the Debye-temperature,  $E_{iz}$  the energy corresponding to the  $z$ -component of the incident wave vector, and  $T$  the surface temperature (refer Section 2.1.2 for details). Since the surface is bulk terminated (see discussion in Section 3.3), the major contribution is expected from Al (bulk Debye temperature is 394 K [130]). In this case, the value of  $2W$  for the parameter range of the present measurements is always greater than 1, suggesting a strong contribution of multiphonon scattering. For the particular spectra presented in Figure 5.1 (see figure caption for experimental parameters), the value of  $2W$  is calculated to be approximately 3.5 (note that the surface Debye

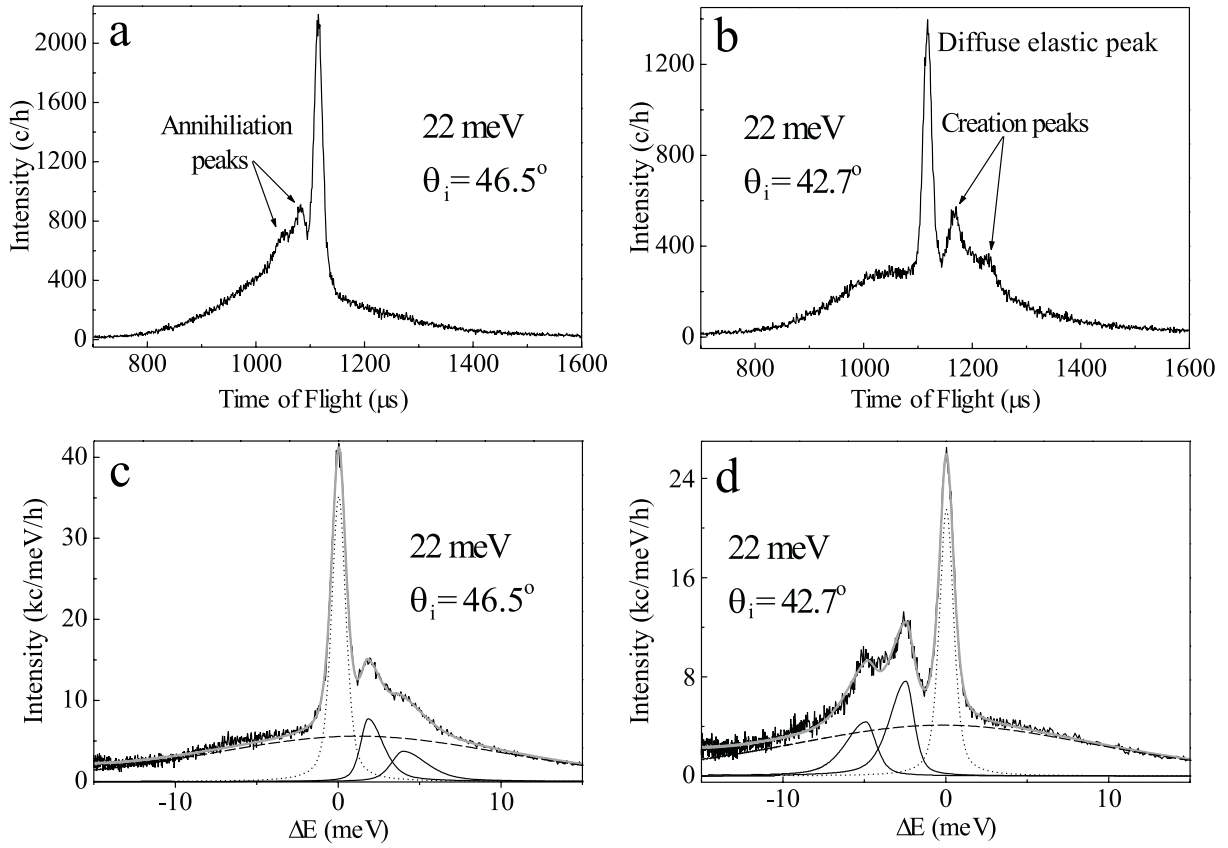


**Figure 5.1:** Representative TOF spectra from the 10-fold surface of  $d\text{-Al}_{71.8}\text{Ni}_{14.8}\text{Co}_{13.4}$  recorded at  $\theta_i = 46.5^\circ$  (a) and  $42.7^\circ$  (b) for the  $[001\bar{1}0]$  azimuth and the sample temperature of around 200 °C. (c) and (d): the intensity versus phonon energy transfer. (Solid gray curve: total fit, solid curve: phonon peak, dotted curve: elastic peak, dashed curve: background.)

temperature is roughly equal to the bulk Debye temperature times  $1/\sqrt{2}$  [149]).

The inelastic intensities resulting from multiphonon scattering normally appear underneath the single phonon peaks as background [114]. On the other hand, the contribution from the bulk phonons is also expected in the measured TOF spectra because there exists a continuum of surface projected bulk bands very close to the Rayleigh modes for a given wavevector, which may also appear as a broad background in TOF spectra. The observed background intensity in the measured TOF spectra could be the contribution from the both multiple surface phonon and the continuum of bulk phonons.

### TOF Spectra at Different Sample Temperatures

TOF spectra were recorded at different sample temperatures ranging from room temperature to 550 °C to investigate the temperature dependence of the different contributions of the TOF spectra. A set of spectra for selected temperatures (beam energy 22 meV and  $\theta_i = 43^\circ$ ) is given in Figure 5.2. The phonon peaks do not shift with temperature. This reveals that the sound velocity does not change appreciably with temperature at least up to 550 °C.

The different components of the TOF spectrum behave differently with temperature. As expected the intensity of the diffuse elastic peak decays exponentially (Figure 5.3, left) with a decay constant of  $\alpha \sim 0.006 \text{ K}^{-1}$ . The decay is identical to that for the specular peak (see comparison in figure). The surface Debye temperature is estimated about 335 K from the decay constant considering only aluminum atoms on the topmost surface layer. The bulk Debye temperature of 394 K yields a surface Debye temperature of around 280 K, which is smaller than the value calculated from the experimental attenuation by almost 20 %. It should be mentioned that the presented sample temperatures were extrapolated from a reference temperature at

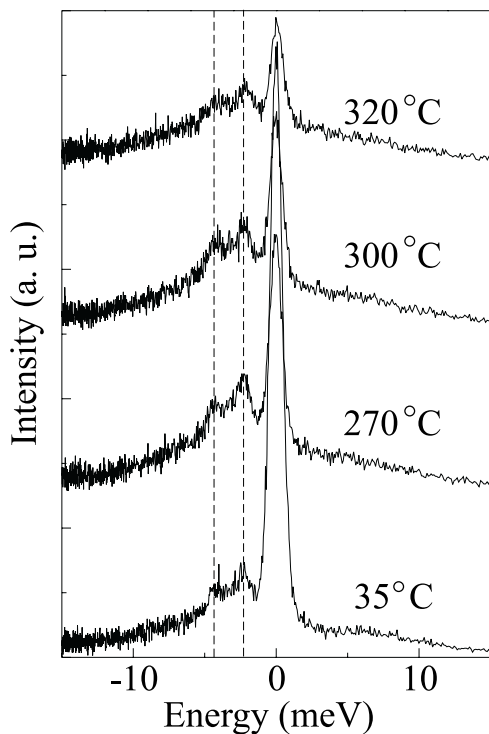


**Figure 5.2:** TOF spectra at selected sample temperatures. Sample temperatures are shown above the spectra. The spectra are recorded along the  $[001\bar{1}0]$  azimuth at  $\theta_i = 43^\circ$  with 22 meV beam energy.

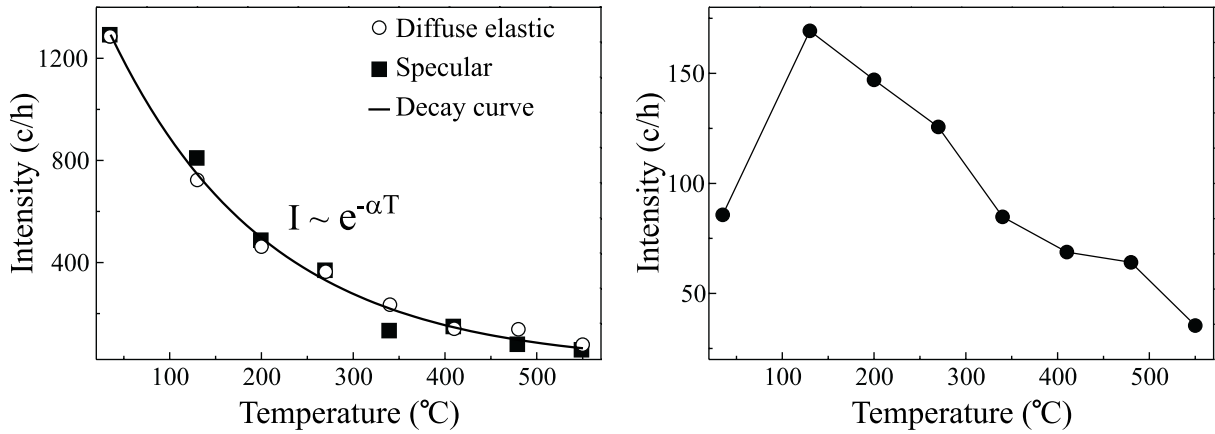


**Figure 5.3:** Left: the intensity as a function of sample temperature for the diffuse elastic peak (open circles) and for the specular peak (solid squares). The specular intensity has been multiplied by a factor of  $1/200$ . The solid curve represents a fit with an exponential decay. Right: the phonon intensity as a function of temperature.

which the sample starts to glow and were not measured exactly. This may be one of the reasons for the larger error.

The intensity of the phonon peaks increases first, reaches a maximum at around 150-200 °C, and starts to fall off (Figure 5.3, right). For temperature higher than 550 °C, the phonon peaks completely merge into the background.

## 5.2 Dispersion Relation

A set of TOF spectra along the two inequivalent high symmetry directions (see Figure 5.5 for the introduction of the high symmetry directions) for different angles of incidence  $\theta_i$  recorded at 22 meV beam energy and sample temperature of 200°C are shown in Figure 5.4. The positions of single phonon peaks are marked by vertical lines.

An additional peak in the topmost spectrum of Figure 5.4, left (indicated by an arrow) is not due to single phonon scattering. The angle at which the TOF spectrum is measured is very close to a diffraction peak at  $52.6^\circ$  ( $\Delta k_{\parallel} = 1.02 \text{ \AA}^{-1}$ ). The diffraction peak contains a broad, low intensity tail derived from the velocity distribution of incident beam which causes the appearance of the additional elastic peak, a so-called decepton (refer to Section 2.1 for a description of decepton).

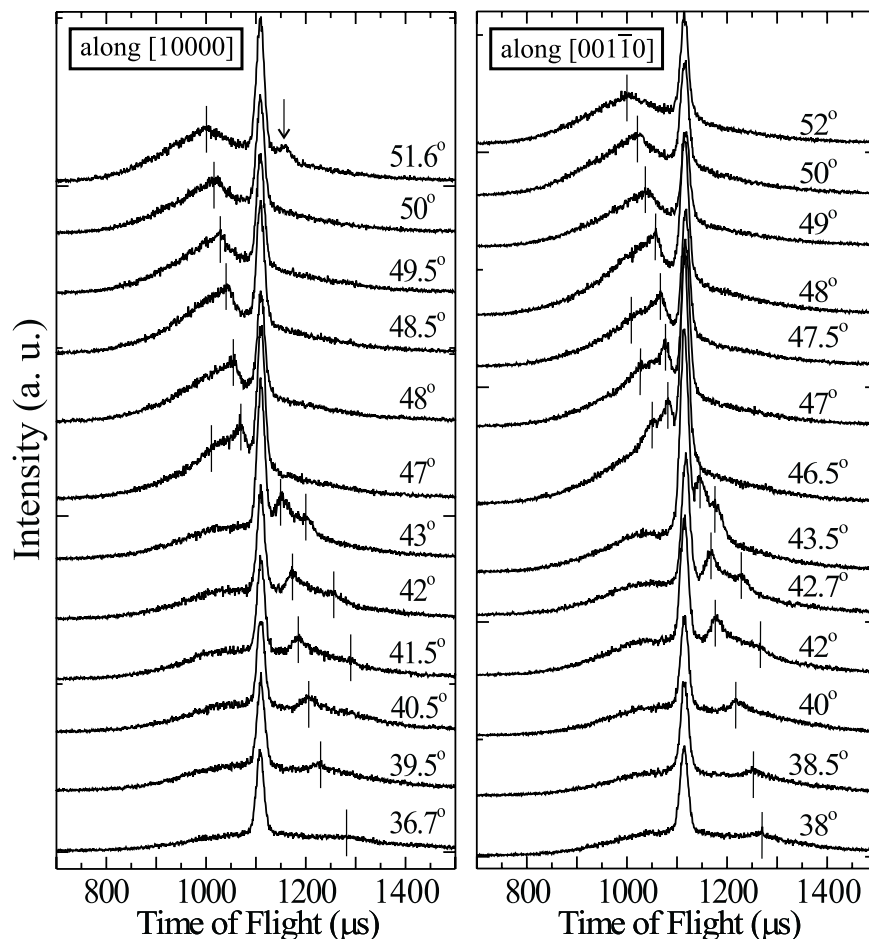


**Figure 5.4:** A series of TOF spectra along the [10000] (left) and [001 $\bar{1}$ 0] (right) azimuth with 22 meV beam energy for different angles of incidence and sample temperature of around 200 °C. Angles are given above the spectra. The positions of single phonon peaks are marked by vertical lines. The peak indicated by an arrow is a decepton.

Figure 5.5 presents the He diffraction pattern of the surface perpendicular to the 10-fold axis. The position and intensity of the spots along the two high symmetry directions are determined from the measured line scans at 22 meV beam energy (see line scans in Figure 3.8). The whole 2D pattern is obtained by symmetrization.

Along the [10000] azimuth, the peaks at  $1.02 \text{ \AA}^{-1}$  (C) and  $1.65 \text{ \AA}^{-1}$  (E) are strongest, while the strongest peaks along [001 $\bar{1}$ 0] are at  $1.2 \text{ \AA}^{-1}$  (G) and  $1.94 \text{ \AA}^{-1}$  (I). The main QBZ boundaries are thus expected at the midpoint of AC, CE, AG, and GI (marked by crosses) and the QBZ centers at the positions of the strongest peaks.

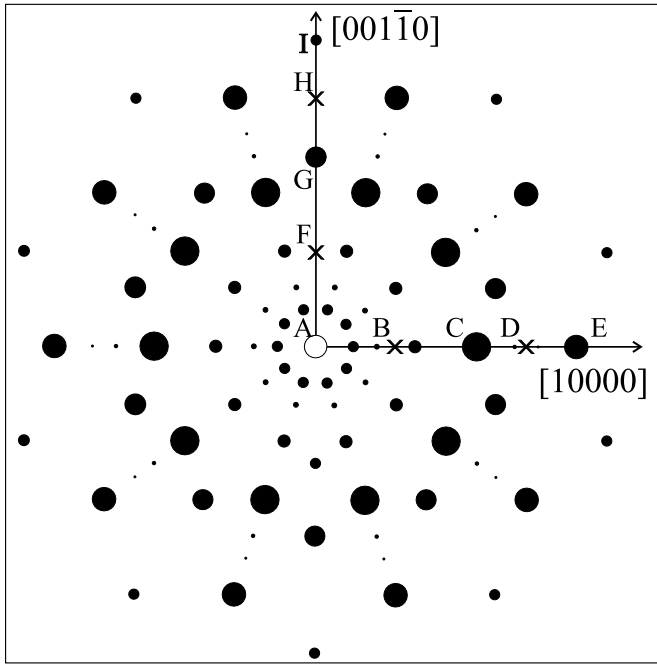


**Figure 5.5:** He diffraction of the 10-fold *d*-Al-Ni-Co surface represented by solid circles. The radius of circles is proportional to the intensity (note the specular intensity is not scaled). The high symmetry points of the QBZs are denoted by letters A, B, C,... and the points marked by crosses are the QBZ boundaries.

The resulting dispersion relations from the sets of measured TOF spectra at different beam energies from 10-33 meV are shown in Figure 5.6. Due to the lack of periodicity, the reduced BZ scheme to express the dispersion relation is not meaningful in quasicrystals. The dispersion curve folded in the first quadrant of  $(\omega, k)$  space is illustrated in Figure 5.7. The QBZ centers and boundaries are marked by the letters given in Figure 5.5.

In the long wavelength limit, the low energy vibrations in solids are sound waves with a linear dispersion relation  $\omega_{l,t} = v_{l,t}k$ , where  $v_l$  and  $v_t$  are the velocities corresponding to the longitudinal and transverse sound waves. Thus, the slope of the linear dispersion yields the sound velocity. The slope of the solid lines shown in Figures 5.6 and 5.7 is determined from the velocity  $v_R$  of the Rayleigh mode estimated from the bulk velocities of *d*-Al-Ni-Co by using a relation  $v_R/v_t = (0.87 + 1.12\sigma)/(1 + \sigma)$  with  $\sigma = (1 - 2v_t^2/v_l^2)/2(1 - v_t^2/v_l^2)$ , which is obtained by an approximation for an isotropic elastic medium [150]. Since *d*-Al-Ni-Co is found to be elastically isotropic [151], the relation can be employed in our system. Neutron scattering from the *d*-Al-Ni-Co yields  $v_l = 7000 \pm 150$  m/s and  $v_t = 4100 \pm 150$  m/s. Using these values,  $v_R$  is estimated  $3750 \pm 5\%$  m/s. This isotropic sound velocity is used for the solid lines giving the bulk derived linear dispersion along the [10000] and [001 $\bar{1}$ 0] directions in Figures 5.6 and 5.7.

As seen, clearly the measured dispersion curves hold a linear relation following the bulk

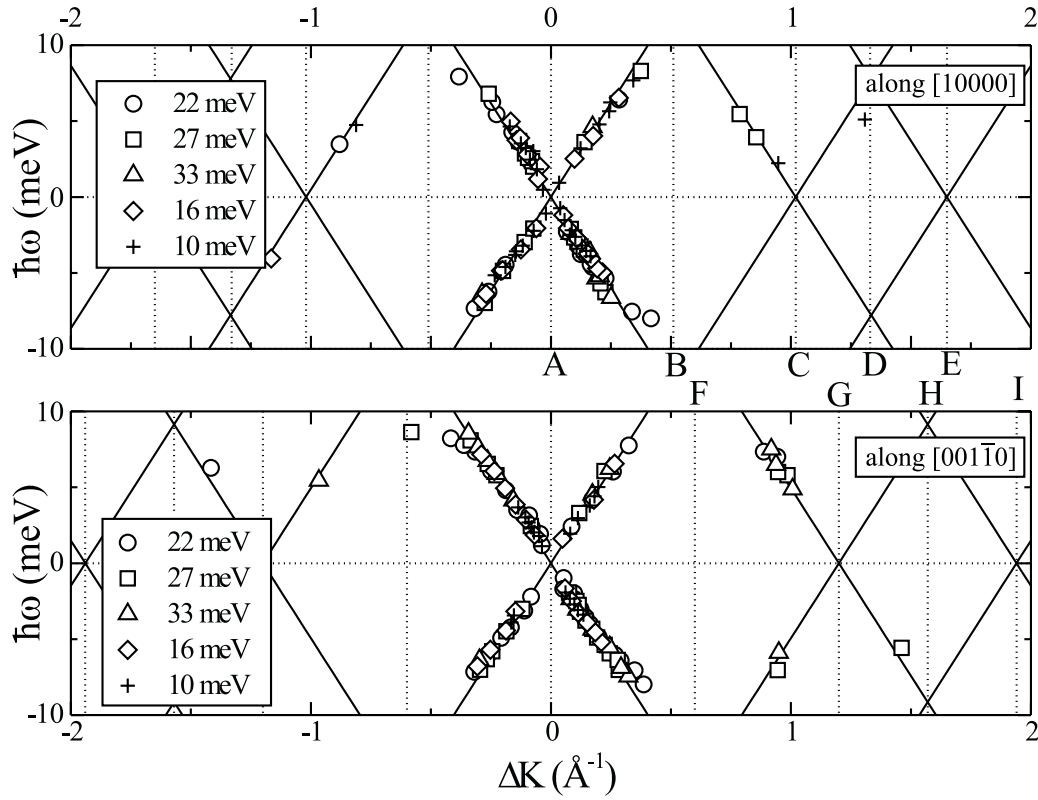


**Figure 5.6:** The phonon dispersion relation along  $[10000]$  (upper) and  $[001\bar{1}0]$  azimuth (lower). Different symbols represent the data obtained for different beam energy. The solid lines represent the linear dispersion expected from the bulk ( $v_R = 3750$  m/s).

expected dispersion curves originating from the QBZ centers up to a certain wavevector. For both high symmetry directions, the linearity holds up to around  $0.30 \text{ \AA}^{-1}$  (energy 7.5 meV). This observation is quite similar to bulk phonon dispersion which also shows a linear relation up to this wavevector [72]. Strong phonon peaks are observed in the dispersion curves close to the Bragg peaks. Although no phonons are detected near the QBZ boundaries, the acoustic mode follows the expected dispersion leveling off towards these points.

The opening of a gap were intensively searched for by varying all possible experimental parameters. However, no indication of gaps were found. Phonon peaks are very broad for higher energy such that it is very hard to separate them from the background. Finding the gaps is almost impossible as the dispersion curves do not clearly extend up to the QBZ boundaries.

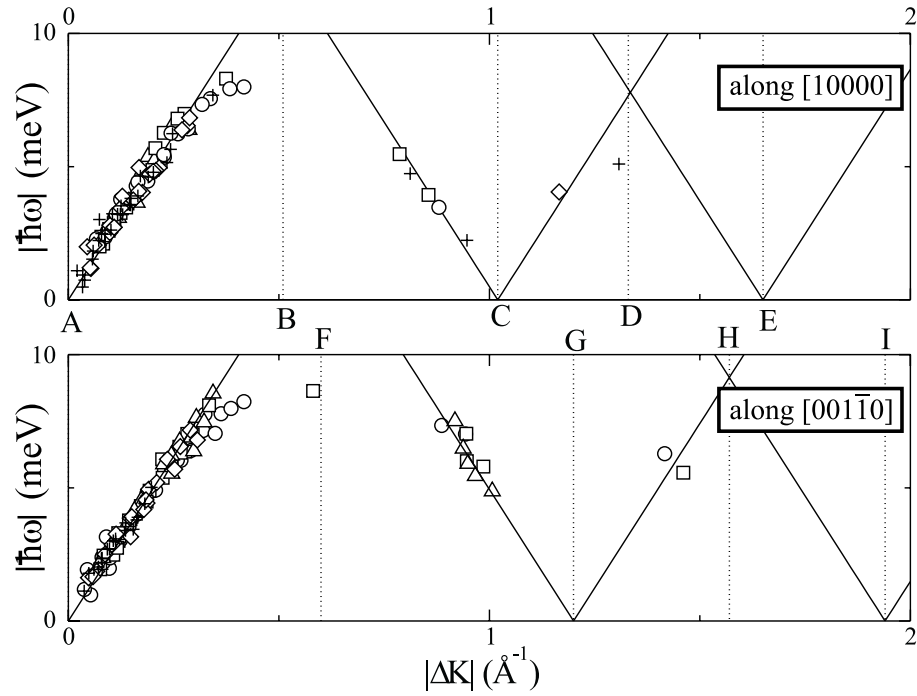


**Figure 5.7:** The dispersion curves folded in the first quadrant of  $(\omega, k)$  space along  $[10000]$  (upper) and  $[001\bar{1}0]$  azimuth (lower). Symbols are as Figure 5.6.

### 5.3 Phonon Peak Width

As discussed in the beginning of this chapter, the investigations of the bulk phonons reveal that the phonon peak width is limited by instrumental resolution up to a certain wavevector and increases rapidly with larger wavevector. To determine whether the surface phonons show a similar behavior, experimental TOF spectra are analyzed in detail, which is presented in this section. For the analysis, the peaks attributed to phonon creation are chosen. As the energy resolution strongly depends on energy transfer, an optimum energy resolution can be achieved in the creation peaks (see Section 2.1.4 for details). The dispersion relation for the selected peaks is shown in Figure 5.8, top (beam energy 22 meV, direction  $[001\bar{1}0]$ ,  $\theta_i = 38^\circ - 43.7^\circ$ ). Below  $\theta_i = 38^\circ$  ( $\Delta K > 0.30 \text{ \AA}^{-1}$ ) the phonon peaks of this branch are very weak such that it is impossible to determine their width reliably.

The peak height as a function of momentum transfer is shown in Figure 5.8, middle. The height is determined by a fit of the TOF spectra as described in the previous section. Since the TOF spectra to which the peaks under discussion belong were recorded under different sample

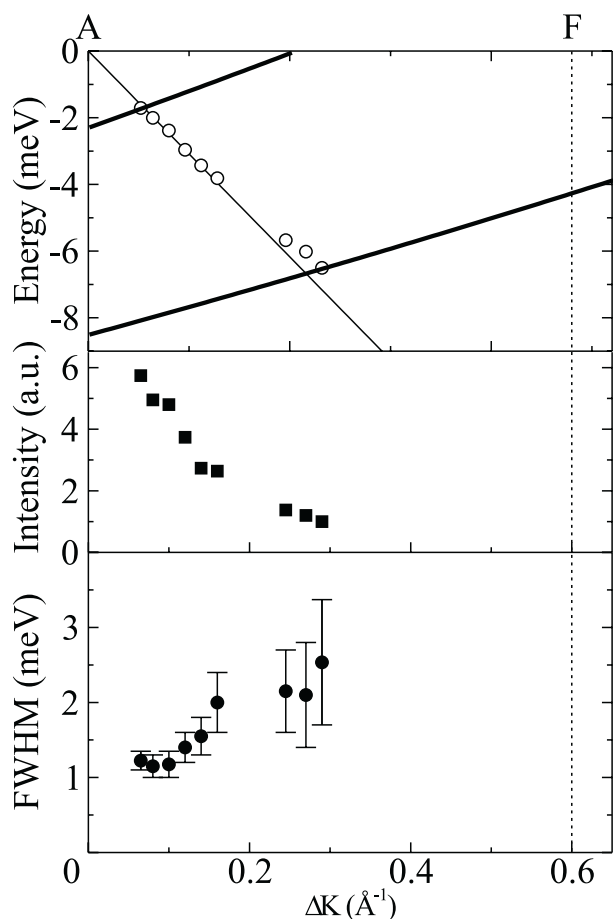


**Figure 5.8:** Top: The dispersion relation with scan curves (thick solid line) for selected peaks. Middle: Phonon peak height as a function of phonon wavevector. Bottom: the full-width at half-maxima for selected peaks.

conditions, the peak heights are rescaled based on the intensity of the diffuse elastic peak. The plot of peak height versus wavevector shows a monotonic decrease in agreement with expected behavior discussed in Section 2.1.2. The strong decrease in peak height results in a less accurate peak width determination at larger wavevectors. The data can be fitted within a reasonable statistical error for a fairly wide range of the peak width. Exemplary for the selected TOF spectra, those with phonon peaks at  $\Delta K = 0.12 \text{ \AA}^{-1}$  and  $0.29 \text{ \AA}^{-1}$  (TOF spectra at  $\theta_i = 42^\circ$  and  $38^\circ$ , respectively) are shown in Figure 5.9. At lower wavevector, the phonon peaks have sufficiently high intensity to determine the width with a relatively small error. In contrast, for larger wavevector the intensity of the peaks is very weak compared to the Gaussian background and the peak shape cannot be determined exactly. For the particular spectrum at  $\theta_i = 38^\circ$ , the full-width at half-maxima (FWHM) can be varied from 1.7 meV to 3.4 meV while maintaining a reasonable agreement of fit and data. The FWHM of the entire data set is given in Figure 5.8, bottom, which demonstrates that average value of the widths increases with increasing

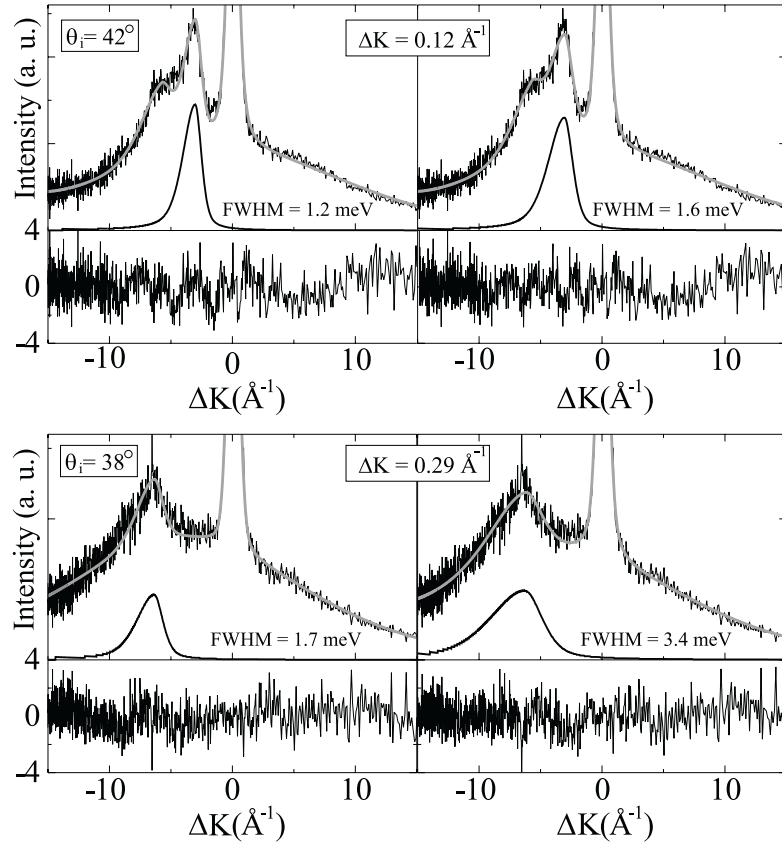


**Figure 5.9:** Demonstration of data fitting to determine peak widths. The upper and lower are the measured TOF spectra at  $\theta_i = 42^\circ$  and  $38^\circ$  with the results of fit (see previous section for the description of fitting procedure). The normalized deviation of fitted curve from the measured data is shown at the bottom of each spectrum. The left and right show the fitting for the lower and upper limit of the width. The upper spectrum is fitted keeping the width of second phonon peak at  $-4.9$  meV the same for the left and right.

wavevector. However, the accuracy of the peak width becomes poor with increasing wavevector.

In addition to the intrinsic broadening, the peak width depends on instrumental broadening as well as on the angle of intersection of the scan curve with the dispersion curve (kinematical focusing, Section 2.1.2). The instrumental broadening is very similar for all peaks under discussion. To consider the effect of kinematical focusing, the scan curves for  $\theta_i = 38^\circ$  and  $43.7^\circ$  are plotted in Figure 5.8, top (refer to Equation 2.37 for the functional dependence of the scan curve on experimental parameters). The angle of intersection does not change appreciably for the TOF spectra under consideration revealing that this contribution is similar for all data.

Hence, the external factors influencing the peak width do not significantly contribute to the  $k$ -dependence of the broadening and the  $k$ -dependence of experimental widths shown in Figure 5.8, bottom reflects changes in intrinsic width.

The bulk phonons (transverse modes) of *d*-Al-Ni-Co show instrumental resolution limited peaks up to a wavevector of around  $0.30 \text{ \AA}^{-1}$  and peak width rapidly increase for larger wavevector [72]. Since the phonon peaks are not separable from the background intensity in the measured TOF spectra for  $\Delta K > 0.29 \text{ \AA}^{-1}$ , a discussion about the peak widths in the wavevector range where the bulk phonons show peak broadening is not possible.

To conclude this section, with all possible experimental parameters and the available capability of the He scattering machine as well as the optimum structural quality of the surface, it is not possible to determine whether the phonon peaks exhibit a strong increase of intrinsic width beyond a specific momentum.

### Summary

The surface is found to possess a well defined Rayleigh mode. The dispersion follows a linear  $k$ -dependence up to a wavevector of  $0.30 \text{ \AA}^{-1}$  giving a sound velocity of about  $3750 \text{ m/s}$  which is isotropic and in good agreement with bulk measurements. Quasi-Brillouin zone centers are identified at the positions of the strong Bragg peaks. The extrapolation of the obtained dispersion relation indicates that the curve becomes dispersionless at the QBZ boundaries. With available instrumental capabilities, the peak broadening as observed in the bulk phonons could neither be confirmed nor be ruled out.